

04.1;12.2

The effect of the target material and the size of the irradiated volume on the efficiency of ozone synthesis in plasma created by pulsed electron beam in air

© D.L. Kuznetsov, Yu.S. Surkov, I.E. Filatov

Institute of Electrophysics, Ural Branch, Russian Academy of Sciences, Yekaterinburg, Russia
E-mail: kdl@iep.uran.ru

Received June 6, 2023

Revised June 22, 2023

Accepted June 29, 2023

The effect of the target material and the size of the irradiated volume on the efficiency of ozone synthesis in air under the action of a pulsed electron beam is investigated. Graphite and lead targets were used. The highest concentration of ozone was observed in a chamber without a target, and the highest specific ozone yield without consideration of electron reflection ($230 \text{ g} \cdot (\text{kW} \cdot \text{h})^{-1}$) was observed in a chamber with a lead target at a minimum air gap (3 cm). The results are explained by the processes of multiple reflection of electrons from elements with a high atomic number at small air gaps compared to the size of the target.

Keywords: pulsed electron beam, ozone synthesis, non-equilibrium plasma, electron reflection.

DOI: 10.61011/TPL.2023.09.56699.19648

Ozone is one of the products of electrophysical processing of oxygen-containing gas mixtures. The method of application of electron beams for ozone synthesis competes with electrical-discharge techniques (when air is irradiated with electron beams, the specific yield of O_3 is as high as $80\text{--}90 \text{ g} \cdot (\text{kW} \cdot \text{h})^{-1}$ [1,2]). Produced ozone may react with the volume either directly [3] or in the presence of catalysts [4,5] and enhance the impact of a beam. If ozone is a by-product of beam processing, its concentration needs to be kept below the threshold limit value [6,7].

In compact setups, an electron beam, which produces nonequilibrium plasma, loses only a fraction of its energy in gas, and the major part of energy is absorbed in the reaction chamber walls. However, electrons may get reflected off the surface and continue moving through gas in a new direction. Therefore, the influence of the size of a reaction chamber and the type of material of its walls on the ozone synthesis efficiency needs to be examined.

The diagram of the setup is shown in Fig. 1. A RADAN-220 electron source with an IMA3-150E electron tube produced a beam of electrons with their maximum and mean energies being equal to 220 and 167.6 keV, a current amplitude of 1 kA, a half-amplitude duration of 1.5 ns, radius $R_t = 0.7 \text{ cm}$ at the foil, and a pulse repetition rate of 7.5 Hz [8]. Electrons were directed into a chamber (steel cylinder with inner radius $R_c = 9.4 \text{ cm}$). A brass flange with an opening limited angle θ between the direction of propagation of primary electrons and the chamber axis to 45° . A $\text{N}_2\text{:O}_2 = 80\text{:}20$ (by volume) gas mixture was used instead of air. Lead (atomic number $Z = 82$) and graphite (carbon has $Z = 6$) targets with a radius of 8.75 cm were mounted inside the chamber. Gap d between the foil and the target could be adjusted within the 3–17 cm range. The ozone concentration was

determined spectrophotometrically [9] using the tables of ozone absorption at a wavelength of 255 nm [10]. The error of determination of the ozone concentration did not exceed 5%.

Air was irradiated with five series of 375 pulses each (1875 pulses in total). The ozone concentration was measured 1, 2, 3, 4, and 5 min after the start of processing. The measurements of $[\text{O}_3]$ were continued for 35 min (in 5 min intervals) after completion of the irradiation procedure.

Experiments were performed at room temperature. Since the mean beam power was low (1.6 W) and an intense heat exchange between the gas mixture, targets, and thick

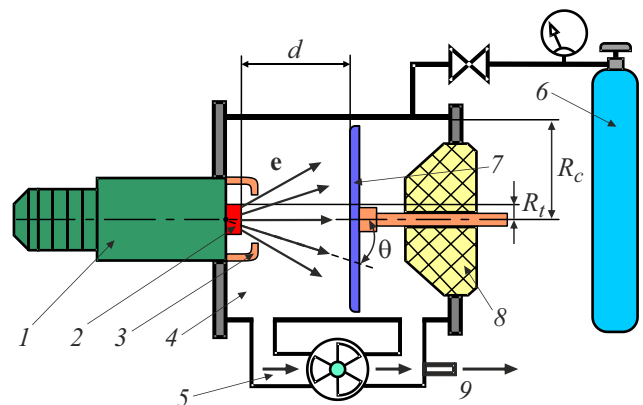


Figure 1. Diagram of the experimental setup. 1 — Compact electron source RADAN-220, 2 — sealed-off electron tube IMA3-150E, 3 — brass flange with an opening, 4 — reaction chamber, 5 — air mixing system needed to obtain a uniform ozone concentration within the chamber volume, 6 — cylinder with a nitrogen–oxygen mixture, 7 — target, 8 — insulator, and 9 — opening for sampling with a syringe.

chamber walls was maintained by the mixing system, no noticeable heating was observed. The temperature of the mixture, targets, and the chamber did not exceed 298 K throughout the entire length of the irradiation sequence (5 min).

It is clear from general considerations that the synthesis of ozone under the influence of an electron beam is affected by five major processes: ozone production under the influence of a beam (process of the zeroth order with respect to concentration) and four first-order ozone loss processes (decomposition under the influence of a beam (with time constant $\tau_{e,b}$), spontaneous decomposition within the chamber volume (τ_v), decomposition at the target (τ_t), and decomposition at the chamber walls (τ_w)). Processes with such dynamics have been examined thoroughly both theoretically and experimentally and are characterized by standard time dependences of the product concentration: it increases exponentially, eventually attaining saturation, under the influence of a beam and decreases exponentially after the completion of irradiation. Only the last three decomposition processes remain in effect after irradiation, and the concentration decreases as $[O_3](t) = [O_3]_{\max} \exp[-g_{dec}t]$, where $[O_3]_{\max}$ is the ozone concentration after 1875 irradiation pulses and $g_{dec} = \tau_v^{-1} + \tau_t^{-1} + \tau_w^{-1}$ is the overall rate constant of ozone decomposition without irradiation. The obtained experimental $[O_3](t)$ dependences are characterized well by the above exponential curves. This verified our assumptions regarding the key ozone synthesis and decomposition processes and provided an opportunity to determine $g_{dec} = 0.0005 \text{ s}^{-1}$ for lead and 0.0016 s^{-1} for graphite. The difference is probably attributable to intense oxidation of carbon by ozone.

All five processes affect the synthesis in the course of irradiation, and the ozone concentration increases as $[O_3](t) = [O_3]_{\text{lim}} \{1 - \exp[-(g_{e,b} + g_{dec})t]\}$, where $[O_3]_{\text{lim}}$ is the limit steady-state ozone concentration and $g_{e,b} = \tau_{e,b}^{-1}$ is the rate constant of ozone decomposition within the irradiated volume under the influence of a beam. Measurements of $[O_3]$ and the obtained g_{dec} values allowed us to calculate $g_{e,b}$. These values are almost independent of the target material, but depend strongly on d : as d increases from 3 to 17 cm, $g_{e,b}$ increases from 0.001 to 0.004 s^{-1} , since a more and more significant fraction of ozone in the chamber is subjected to irradiation.

Figure 2 shows the dependence of $[O_3]_{\max}$ on d for lead and graphite targets and the chamber without a target. Concentrations are normalized to standard conditions. It is evident that $[O_3]_{\max}$ increases from 85 to 170 ppm (for graphite) and from 120 to 205 ppm (for lead) as d varies from 3 to 17 cm. The greatest (1.4-fold) $[O_3]_{\max}$ difference between two targets is observed in the case of small gaps. The extrapolation of $[O_3]_{\max}$ values into the $d = 17 \text{ cm}$ region (dashed sections of curves) reveals that the values for different targets grow closer and become equal at point $d = 28 \text{ cm}$ (this corresponds to the chamber without a target, where $[O_3]_{\max} = 215 \text{ ppm}$). Since the maximum range of electrons with an energy of 167.6 keV in air is

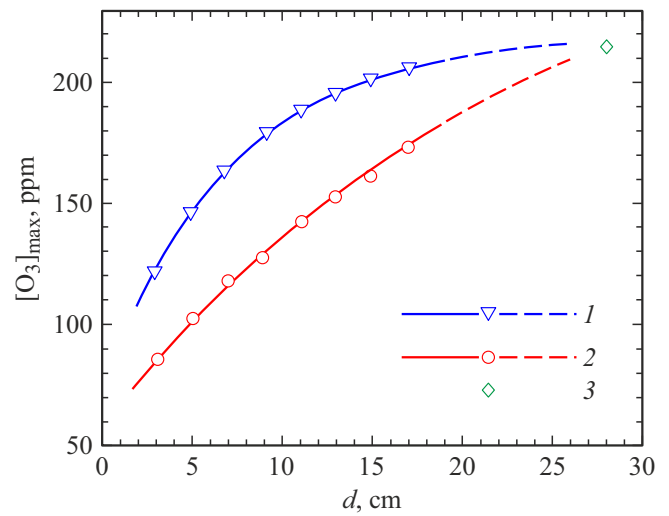


Figure 2. Ozone concentration $[O_3]_{\max}$ after 1875 electron-beam pulses as a function of distance d between the target and the output foil of the electron tube for lead (1) and graphite (2) targets and for the chamber without a target (3).

$\sim 28 \text{ cm}$ [11] and the distance from the tube foil to the insulator is also 28 cm, electrons are absorbed in air and on the side walls of the chamber.

The energy efficiency of ozone synthesis is characterized by specific yield

$$G(O_3) = A[O_3]N_A V_c / [V_m(W_{e,b})_1 N], \quad (1)$$

where $G(O_3)$ is the specific yield of ozone $[\text{g} \cdot (\text{kW} \cdot \text{h})^{-1}]$,

$$A = 1.7909 \cdot 10^{-3} \text{ eV} \cdot \text{g} \cdot (\text{kW} \cdot \text{h} \cdot \text{ppm})^{-1}$$

is the conversion constant, $[O_3]$ is the ozone concentration [ppm],

$$N_A = 6.02214 \cdot 10^{23} \text{ mol}^{-1}$$

is the Avogadro number, $V_c = 9737 \text{ cm}^3$ is the chamber volume, $V_m = 22414 \text{ cm}^3 \cdot \text{mol}^{-1}$ is the molar volume of gas, $(W_{e,b})_1$ is the electron-beam energy in a single pulse [eV], and N is the number of pulses.

For a comparison of specific yields to be correct, one needs to choose such numbers of pulses that provide a fixed ratio of the ozone concentration to limit value $[O_3]_{\text{lim}}$. We chose $N = N_{0.4}$ (i.e., the number of beam pulses producing $[O_3]_{0.4} = 0.4[O_3]_{\text{lim}}$). The values of $N_{0.4}$ vary with d , but inequality $N_{0.4} < 1875$ always holds.

It is convenient to estimate the ozone synthesis efficiency using specific yield $G_f(O_3)$ with respect to the total electron-beam energy in a single pulse

$$(W_{e,b})_{1f} = (\varepsilon_{av}/e) \int I(t)dt,$$

where $\varepsilon_{av} = 1.676 \cdot 10^5 \text{ eV}$ is the mean energy of beam electrons, $e = 1.60218 \cdot 10^{-19} \text{ C}$ is the electron charge, and $\int I(t)dt$ is the total charge of beam electrons in a

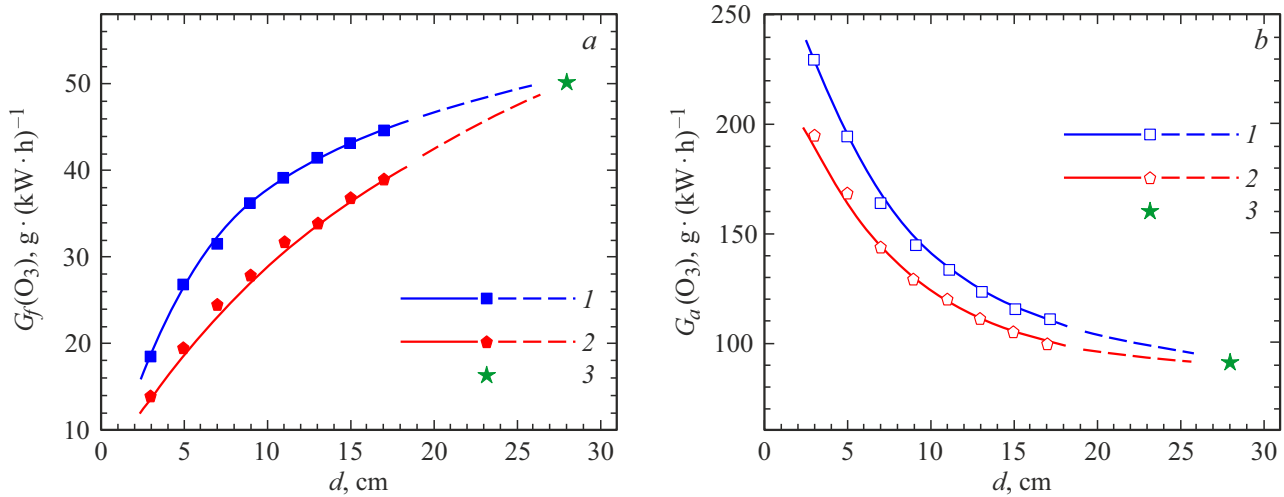


Figure 3. Specific ozone yield with respect to the total electron-beam energy $G_f(O_3)$ (a) and the beam energy absorbed in air $G_a(O_3)$ (b) as a function of distance d between the target and the output foil of the electron tube for lead (1) and graphite (2) targets and for the chamber without a target (3).

pulse [C]. The calculated value is $(W_{e.b})_{1f} = 1.57 \cdot 10^{18}$ eV (0.25 J). Specific yield $G_a(O_3)$ with respect to the beam energy absorbed in air in a single pulse ($(W_{e.b})_{1a}$) is more convenient for analysis of processes in the irradiated volume. One may determine $(W_{e.b})_{1a}$ via numerical integration in spherical coordinates

$$(W_{e.b})_{1a} = [2\pi e(1 - \sqrt{2}/2)]^{-1} \times \int I(t) dt \int_0^{\pi/4} \left[\int_{r_0}^{r_0+l(\theta)} (d\varepsilon/dr) dr \right] \sin \theta d\theta \int_0^{2\pi} d\varphi, \quad (2)$$

where θ is the angle between the direction of electron motion and the chamber axis, $d\varepsilon/dr$ is the specific linear electron energy loss in air [$\text{eV} \cdot \text{cm}^{-1}$], $r_0 = R_t / \cos \theta$ is the distance from the origin of coordinates to the point of electron exit from the foil [cm], and $l(\theta)$ is the length of the electron track in air to the point of collision with the target or the chamber walls [cm]. The data for silicon [11] adjusted in accordance with the density ratio of air and silicon were used to determine $d\varepsilon/dr$. The integral in square brackets represents the integral linear energy loss of an electron with initial energy ε_{av} that traveled over distance $l(\theta)$ in air. The length of this distance was calculated as $l(\theta) = d / \cos \theta$ at $0 \leq \theta \leq \theta_0$ and $l(\theta) = R_c / \sin \theta - r_0$ at $\theta_0 \leq \theta \leq \pi/4$. Here, θ_0 is the smallest angle at which electrons reach the side walls of the chamber (angles θ_0 vary with d). The error of determination of $(W_{e.b})_{1a}$ did not exceed 10%, while the errors of determination of $G_f(O_3)$ and $G_a(O_3)$ were no greater than 15%. Reflections of electrons off the targets and walls were neglected, since it is very difficult to introduce them into calculations. It was decided that the specific yields of ozone for two targets and different gaps determined without regard to reflections would be compared and the

results of this comparison would be used to assess the role of reflection processes in ozone synthesis.

Figure 3, a shows the dependences of specific ozone yield $G_f(O_3)$ on d . As d increases from 3 to 17 cm, $G_f(O_3)$ grows from 14 to 39 $\text{g} \cdot (\text{kW} \cdot \text{h})^{-1}$ for graphite and from 19 to 45 $\text{g} \cdot (\text{kW} \cdot \text{h})^{-1}$ for lead. The greatest (as above, 1.4-fold) difference between the $G_f(O_3)$ values for lead and graphite is observed in the case of small gaps; the difference at large d values is less significant. The extrapolation of $G_f(O_3)$ values into the $d > 17$ cm region reveals that the values for different targets grow closer and become equal ($50 \text{ g} \cdot (\text{kW} \cdot \text{h})^{-1}$) at point $d = 28$ cm, which corresponds to the chamber without a target.

The dependences of specific ozone yield $G_a(O_3)$ on d are shown in Fig. 3, b. They differ from those presented in Fig. 3, a. As d increases, $G_a(O_3)$ decreases from 195 to 100 $\text{g} \cdot (\text{kW} \cdot \text{h})^{-1}$ for graphite and from 230 to 110 $\text{g} \cdot (\text{kW} \cdot \text{h})^{-1}$ for lead. The greatest positive difference between the $G_a(O_3)$ values for lead and those for graphite is observed at $d = 3$ cm. The extrapolation of $G_a(O_3)$ values into the $d > 17$ cm region also reveals that the values for different targets grow closer and become equal ($95 \text{ g} \cdot (\text{kW} \cdot \text{h})^{-1}$) at point $d = 28$ cm for the chamber without a target. It was assumed that $G_a(O_3)$ should not decrease with increasing gap width, since the ozone concentration should grow alongside with the increase in energy deposition into air. However, when d grew from 3 to 28 cm in experiments, the fraction of the beam energy absorbed in air (calculated without regard to reflections) increased from 8 to 54%, while $[O_3]$ increased only by a factor of 2–2.5. It is known [12] that the coefficient of reflection of electrons off the surface of lead at $\theta = 0$ – 45° is ~ 0.5 – 0.6 and is 4–8 times greater than the corresponding coefficient for graphite. Since a brass flange is positioned in the chamber opposite the target, electrons reflected

off the target may also get reflected off the flange (with a coefficient of $\sim 0.3\text{--}0.4$), i.e., multiple reflection of electrons and, consequently, a significant increase in electron energy losses in air are possible. In the case of small gaps, the process of multiple reflection may enhance the energy deposition into air by a factor of 2–2.5. Owing to a complex angular distribution of reflected electrons, the probability of multiple reflection decreases with increasing gap width. As the gap width increases, an increase in irradiated volume coupled with a simultaneous reduction in energy contribution of multiply reflected electrons stabilize the values of $G_a(\text{O}_3)$ determined with account for reflection, and these values vary weakly with d , falling within the interval of $90\text{--}100 \text{ g} \cdot (\text{kW} \cdot \text{h})^{-1}$ for both types of targets.

Thus, it was found experimentally that electrons reflected off a target play a significant part in the process of ozone synthesis in air under the influence of a pulsed electron beam. Their effect is the strongest in the case of air gaps being considerably smaller in size than the targets that are themselves made of materials with large atomic numbers. The obtained results may be applied in the design of both facilities for ozone synthesis in air under electron-beam irradiation and process facilities where ozone is an unwanted by-product.

Conflict of interest

The authors declare that they have no conflict of interest.

References

- [1] M.R. Cleland, R.A. Galloway, *Phys. Procedia*, **66**, 586 (2015). DOI: 10.1016/j.phpro.2015.05.078
- [2] Y.A. Kotov, S.Y. Sokovnin, *IEEE Trans. Plasma Sci.*, **28** (1), 133 (2000). DOI: 10.1109/27.842883
- [3] K. Yang, K. Li, L. Pan, X. Luo, L. Wang, R. Wang, Y. Zhai, Z. Chen, J. Wang, J. Zing, *Toxins*, **12** (2), 138 (2020). DOI: 10.3390/toxins12020138
- [4] T.I. Poznyak, I.C. Oria, A.S. Poznyak, *Ozonation and biodegradation in environmental engineering* (Elsevier, 2019), p. 325–349. DOI: 10.1016/B978-0-12-812847-3.00021-4
- [5] I. Filatov, V. Uvarin, D. Kuznetsov, in *2020 7th Int. Congress on energy fluxes and radiation effects* (EFRE) (IEEE, 2020), p. 317. DOI: 10.1109/EFRE47760.2020.9242056
- [6] S. Barshan, A. Pazirandeh, G. Jahanfarnia, *J. Instrum.*, **15** (1), P01004 (2020). DOI: 10.1088/1748-0221/15/01/P01004
- [7] N. Hara, J. Oobuchi, A. Isobe, S. Sugimoto, J. Takatsu, K. Sasai, *Rad. Oncol.*, **17** (1), 39 (2022). DOI: 10.1186/s13014-022-02005-6
- [8] V.G. Shpak, S.A. Shunailov, M.I. Yalandin, *J. Phys.: Conf. Ser.*, **2064**, 012002 (2021). DOI: 10.1088/1742-6596/2064/1/012002
- [9] I.E. Filatov, V.V. Uvarin, D.L. Kuznetsov, *Tech. Phys. Lett.*, **46** (1), 94 (2020). DOI: 10.1134/S1063785020010216
- [10] L.T. Molina, *J. Geophys. Res.: Atmospheres*, **91** (D13), 14501 (1986). DOI: 10.1029/JD091iD13p14501
- [11] J.B. Marion, F.C. Young, *Nuclear reaction analysis: graphs and tables* (North Holland Publ. Co., Amsterdam, 1968), p. 20–21.
- [12] J.I. Goldstein, H. Yakowitz, D.E. Newbury, E. Lifshin, J.W. Colby, J.R. Coleman, *Practical scanning electron microscopy: electron and ion microprobe analysis* (Plenum Press, N.Y., 1975), p. 49–68.

Translated by Ego Translating